Adaptive Collaborative Position Control of a Tendon-Driven Robotic Finger

Omer Saleem*, Faisal Abbas*, Muhammad Usman Khan*, Muhammad Anas Imtiaz*, Salman Khalid**

** Electrical Engineering Department, National University of Computer and Emerging Sciences, Lahore, Pakistan (e-mail: omer.saleem, abbas.faisal, usman.muhammad@nu.edu.pk, anas_imtiaz@yahoo.com)*
*** BiSMiL Lab, Information Technology University, Lahore, Pakistan (e-mail: m.salmankhalid29@gmail.com)*

Abstract: This paper presents a collaborative control scheme that adaptively combines two different control strategies in order to optimize the trajectory-tracking performance and the angular-position response of the motor, installed at the metacarpophalangeal joint of each finger, in a robotic hand. The scheme contains an adaptive neuro-fuzzy inference system (ANFIS) in the feed-forward path, and a proportional-integral-derivative (PID) controller in the feedback path. The ANFIS supervises the motion-control and efficiently tracks the reference trajectory. The PID controller improves the transient response and robustly nullifies the effects of exogenous disturbances. The final control output is taken as the weighted sum of individual outputs from the ANFIS and PID controller. A hyperbolic tangent function (HTF) of the error dynamics is used to adaptively vary the weightages in the controller combination. This feature dynamically varies the contributions of individual control effort, delivered by ANFIS and PID controller, with respect to the variations in the angular-error dynamics. The PID parameters and the variation-rate of HTF are meta-heuristically tuned via an adaptive particle swarm optimization (APSO) algorithm. The collaborative controller effectively tracks the desired trajectory and improves the overall system response. The results of real-time experiments are presented to validate the efficacy of the proposed controller.

Keywords: Robotic finger, joint-angle response, adaptive controller combination, ANFIS, PID controller, hyperbolic tangent function.

1. INTRODUCTION

The five-fingered robotic hands (FFRH) are capable of imitating the human hand movements. Control of FFRH requires the robotic finger-joints to precisely track the input trajectory patterns. Various designs of anthropomorphic robotic arms are presented in (Carbone and Ceccarelli, 2008; Chen et al., 2012; Xu et al., 2012).

An optimized tracking control system can help improve the agility and flexibility of these end-effectors and allows for dexterous grasping and manipulation of objects, especially in tele-operation applications. Hence, in this paper, an adaptive collaborative position controller (ACPC) is presented to improve the transient and steady-state response of the joint-angle of a robotic finger, even in the presence of rapidly changing reference inputs or bounded disturbances. A lot of work has been done in the past to develop novel and innovative tracking control schemes for robotic hands (Chen and Naidu, 2011; Niehues et al., 2014). Hybrid tracking control strategies offer the best attributes of the different controllers that are being utilized by them (Chen and Naidu, 2013). Therefore, the proposed control scheme adaptively combines the control outputs of a classical feedback controller and an intelligent feed-forward controller, to achieve an optimal overall control performance. The feed-forward controller ensures efficient and accurate tracking of time-varying reference input signals. An intelligent feed-forward controller is thus used to actuate the robotic finger joints according to the position input provided by the trajectory generator (Rezaeeian et al., 2008). The studies show that the ANFIS is a superior intelligent control mechanism than the fuzzy logic or the artificial neural controllers. It adaptively combines the inference and learning based features of both controllers, respectively (Carbureanu, 2014; Potluri et al., 2010; Saini and Rani, 2012; Zaki et al., 2010). In this research, the ANFIS acts as a well-postulated inverse model to the system by simply generating the necessary motor control commands needed to efficiently bring it to the desired position (Duka, 2015).

The generic PID controller is utilized as the feedback position controller. It serves to minimize the tracking error in angular position of the finger joint and improves the transient response of the system. The PID controllers are widely used in process control industry and robotics (Bequette, 2003; Bhatti et al., 2015; Shauri et al., 2014). It is a model-free control mechanism that depends on the weighted sum of the error, its rate-of-change and recent sum (integral). This linear combination of error-dynamics offers a simple yet a reliable and an efficient control strategy. The weightages of the error-dynamics (used in the PID control law) are denoted as the PID parameters. These parameters must be tuned properly to ensure effective control effort delivery. The conventional techniques used to tune these parameters do not always yield the best solution. The meta-heuristic search and optimization algorithms offer a better alternative solution (Vijayakumar and Manigandan, 2016). They search through the provided random population of candidate solutions and stochastically evolve to converge to the global-best solution at a reasonable rate. This property improves the controller performance by optimally tuning the controller parameters. Rigorous research has been done on tuning the PID controllers via genetic, particle swarm, ant-bee colony, and bacterial foraging optimization algorithm etc. (Anbarasi and Muralidharan, 2016; Ghosh and Banerjee, 2015). The particle swarm optimization (PSO) algorithm, and its modified variants, offer relatively faster rate of convergence towards the best-fit solution and are relatively simpler to compute (Biswas et al., 2014; Devaraj, 2015; Medewar and Munje, 2015). Therefore, in this research, the APSO algorithm discussed in (Djoewahir et al., 2013) has been used due its effectiveness in motor control applications. An optimally tuned PID controller quickly nullifies the error, reduces the rise-time and dampens the oscillations in the response. The control mechanism is further enhanced by the addition of tracking-differentiators (TD) in it (Yu and Honglun, 2015; Jun and Huiqiang, 2015; Sharma et al., 2016). The TD enhances the differential-signal quality of the reference as well as the measured signal.

The outputs of the conventional ANFIS and PID controller are subjected to the process of weighted summation. This technique optimizes the overall control output by delivering the best features of both controllers. However, if fixed weightages are used in their combination, the system response tends to exhibit random and abrupt perturbations. Therefore, a predefined rule is needed to change the weightages dynamically with respect to variations in the error dynamics of the joint-angle. Hence, a non-linear function of error is utilized to adaptively vary the weightages of individual control outputs such that when the error (and rate-of-change of error) is large, then the contribution of the PID control effort is increased accordingly. Similarly, when the error is negligible, the control effort delivered by ANFIS is given more weightage. This way, the best performance is achieved from the controller. The final control output (u) provides the excitation voltage required to actuate the motor. Several options of non-linear functions are available in literature; such as sigmoidal, hyperbolic, Guassian, and piece-wise non-linear functions (Salim et al., 2014; Seraji, 1998; Su et al., 2005). However, in this research, a hyperbolic-tangent function (HTF) of error is used (Jimenez-Uribe et al., 2015), restricted within the interval [0, 1]. It is simply a re-scaled sigmoidal function and is, hence, monotonic and differentiable.

The rest of the paper is formatted as follows: Section 2 presents the experimental setup used to test the developed ACPC mechanism on the robotic finger. The finger kinematics and actuator model are presented in section 3. The control system design is explained in section 4. Section 5 presents the real-time experimental tests and their results to evaluate the performance of the proposed control scheme. Section 5 concludes the paper.

2. EXPERIMENTAL SETUP

The robotic hand contains five fingers. Each finger is actuated with the aid of a mini permanent magnet direct-current (PMDC) geared motor. Rotary encoders are used to acquire the information regarding the instantaneous position of the motor shaft, and hence the joint-angle. The finalized position control commands are applied to the robotic finger's joint-motor via a dedicated motor driver circuit.

2.1 Software architecture

A LABVIEW based graphical user interface (GUI), running on a personal computer, is used in this research (Elmerabete et al., 2010). It is used to apply the reference input signal, visualize the corresponding joint-angle response, run the control-routine accordingly, and generate appropriate control signals to improve the system's performance. In order to conduct the "hardware-in-the-loop" simulations, a device is needed to relay the information regarding the position of the joint-motor from the encoders to the GUI, as well as to communicate the string of control signals issued by the software to the motor driver circuit that is actuating the joint-motor. Hence, an 8-bit embedded microcontroller is interfaced with the GUI software to measure the response and accordingly control the position of the robotic finger-joint in real-time. Initially, the reference input signals are fed to TD. The corresponding outputs are fed simultaneously to the ANFIS (as its inputs), as well as to the PID controller for comparison and computation of tracking error. The measured joint-angle, acquired by the microcontroller via the encoders, is serially transmitted (at 9600 bps) to the LABVIEW application. Tracking-differentiation is applied to the received joint-angle data as well. This information is compared with the reference inputs. The corresponding errors are evaluated and fed to the PID control routine. The resulting outputs of ANFIS and PID controller are adaptively fused together. The fused output is transmitted to the microcontroller where it is translated to generate an appropriate pulse-width-modulated (PWM) command. The entire system is operated at a sampling frequency of 250 Hz.

2.2 Embodiment design

The robotic hand has five fingers with one degree-of-freedom in each finger. The motors are installed at the metacarpophalangeal joint of each finger. A tendon-driven (wire-pulley) mechanism is used, in conjunction with the joint-motor, to bend or stretch each finger. The motors offer sufficient driving torque at low rotational speed, have a compact size, and are light in weight. One complete finger, equipped with the wire pulley mechanism, is shown in Fig. 1. The entire structure is fabricated with a 5.0 mm think fiber-glass sheet because it is durable, light-weight and cheap.

Fig. 1. Structure of robotic finger

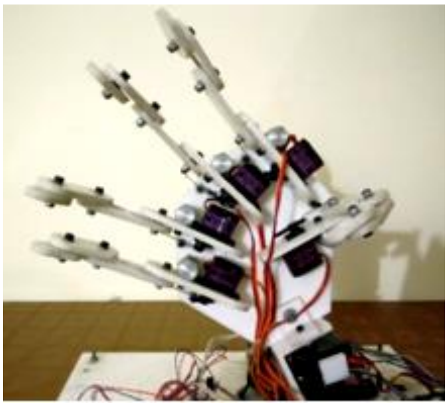

Fig. 2. Five-fingered robotic hand

The fully fabricated structure of mechanical hand is shown in Fig. 2.

3. DYNAMICS OF ROBOTIC FINGER

In this section, the motion of the proposed robotic finger mechanism is analyzed. These dynamics are explained in terms of the kinematics of the finger-joint and mathematical model of the motor that is responsible for rotating the joint.

3.1 Finger kinematics

The schematic of the tendon-driven robotic finger-joint is represented in Fig. 3. Consider the equation of motion, given in (1), for the robotic finger (Abdallah et al., 2013). For this research, zero external forces are assumed.

$$M\ddot{\theta} + \gamma = \tau \tag{1}$$

where,

- M is the joint-inertia
- γ is the sum of the Coriolus, centripetal, gravitational, and frictional forces
- $\ddot{\theta}$ is the angular acceleration of the revolute joint
- τ is the torque applied to the revolute joint

The relationship between τ and the corresponding tension (f) in the tendon is given by (2).

$$\tau = rf \tag{2}$$

where, r is the radius f the joint. The tension is proportional is proportional to the length of the tendon (l), as given in (3). The stiffness-value (k_t) serves as the constant of proportionality.

$$f = k_t l \tag{3}$$

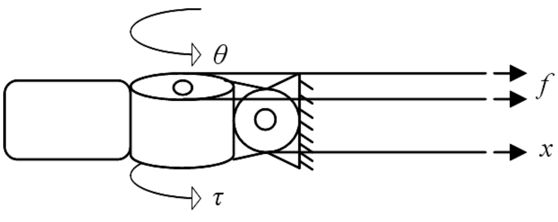

Fig. 3. Schematic of a tendon-driven robotic finger

The resulting position of the tendon (x) is given by (4).

$$x = r\theta + l \tag{4}$$

where, θ is the angular-position of the revolute joint. Substituting the information provided by (2), (3), and (4) in the equation of motion represented by (1), provides the relationship given in (5)

$$x = \frac{1}{rk_t}\left(M\ddot{\theta} + \gamma\right) + r\theta \tag{5}$$

The relationship clearly manifests that the tendon-position is inversely proportional to the tendon-stiffness (k_t), which is normally a very large value. Consequently, the effect of the joint-inertia and the sum of other forces (γ) becomes insignificant and, hence, they can be neglected. Therefore, the finalized relationship of the tendon position with other joint dynamics is given by (6).

$$x = r\theta \tag{6}$$

The simplification depicts that controlling the angular-position (θ) of the joint would automatically serve to control the position (x) of the tendon as well.

3.2 Actuator Model

The fingers in the robotic hand are being driven by metal-geared PMDC servo motors (Widhiada et al., 2015). The transfer function of the angular-displacement of this motor with respect to excitation voltage applied to it is presented in (7).

$$\frac{\theta(s)}{V_a(s)} = \frac{nK_a}{s(s^2PL_a + (L_a v + PR_a)s + R_a v + K_a K_b)} \tag{7}$$

where,

- θ = Angular displacement of motor shaft, (rad.)
- V_a = Armature voltage, (V)
- P = Moment of inertia referred to motor shaft (J_m) and load shaft (J_L) = 0.02675 kgm^2
- L_a = Armature inductance = 2.7 µH
- R_a = Armature resistance = 2.0 Ω
- v = Viscous friction coefficient referred to motor shaft (f_m) and load shaft (f_L) = 0.42 Nms
- K_a = Motor torque constant = 6.28 kg.cm/A
- K_b = Speed proportionality constant = 13.2 rpm/V
- n = Gear ratio = 16

4. CONTROL SYSTEM DESIGN

The proposed control scheme has two major components. The PID controller serving as the feed-back controller and the ANFIS that acts as the feed-forward controller. The outputs of these controllers are modulated with adaptive weightages and are then added to actuate the joint-motor. The input signal and the measured signal are fed to tracking differentiator to obtain an improved signal quality of its first-order derivatives. The synthesis and evolution of the proposed control scheme is discussed in the following sub-sections.

4.1 Tracking differentiation

Before discussing the proposed control law, it is imperative to elaborate the method used to improve the acquired signal quality. The derivative part of the PID controllers depend on the rate-of-change of error between the reference input signal and system's actual output. The input trajectory patterns used for simulations and testing are usually the non-differentiable waveforms such as square or saw-tooth waves. Simple differentiation of such input patterns causes large over-shoot in the system's response at set-point jumps. Moreover, the output sensor (or encoder) signals are discrete in nature and are usually contaminated with random noise. Simple differentiation of such signals is impractical as it amplifies the random noise. With the loss of signal integrity, even a robust controller fails to optimize the system performance. In order to alleviate these issues, a tracking differentiator (TD) is used (Guo et al., 2012). The TD provides two outputs for a given input signal, $\theta(t)$, as shown in (8).

$$\theta_1(t) = \theta(t) \text{ and } \theta_2(t) = \dot{\theta}(t) \tag{8}$$

The non-linear TD structure is given in (9), (10), and (11).

$$\begin{cases} \dot{\theta}_1 = \theta_2 \\ \dot{\theta}_2 = -R\, sat\left(\theta_1 - \theta + \dfrac{|\theta_2|\theta}{2R}, \delta\right) \end{cases} \tag{9}$$

where,

$$sat(x,\delta) = \begin{cases} sign(x) & |x| \geq \delta \\ \dfrac{x}{\delta} & |x| < \delta \end{cases} \tag{10}$$

such that,

$$sign(x) = \begin{cases} -1 & x < 0 \\ 0 & x = 0 \\ +1 & x > 0 \end{cases} \tag{11}$$

In the proposed research, two TD modules are used; one for the differentiation of the input position signals and the other for measured position signal. Each module takes the joint-angle (θ) as the basic input and provides θ and $\dot{\theta}$ (the angular-velocity) at the output.

4.2 Classical feedback controller

The classical feedback controller offers a formidable solution to minimize the tracking error in the angular position (θ) of the joint-motor in the robotic finger. Apart from minimizing the angular-position error, the optimally tuned PID controller also serves to improve the system's transient response by dampening the oscillations, reducing the overshoot, and reducing the rise time.

The PID controller is one of the most widely used model-free controllers in the process-control industry. It is a conventional and linear control mechanism that does not require the mathematical model of the system for its computation.

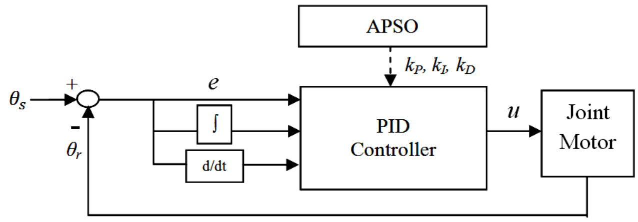

Fig. 4. APSO-tuned PID controller

Despite having a simple structure, it offers effective control effort in bringing the system to its steady-state efficiently. The PID control law is given by (12). The position-error, $e(t)$, is given by (13).

$$u_1(t) = k_P.e(t) + k_I \int_0^t e(\tau)\, d\tau + k_D \left(\frac{d}{dt} e(t)\right) \tag{12}$$

$$e(t) = \theta_s(t) - \theta_r(t) \tag{13}$$

where, k_P, k_I, k_D, are the proportional, integral and derivative gains of the PID controller, respectively. The optimal tuning of the PID parameters tends to enhance the performance of the controller. Therefore, in this research, these parameters are meta-heuristically tuned via an APSO algorithm. The APSO-tuned PID controller is shown in Fig. 4.

As discussed previously, the TDs are used to remove jitter in the input and measured position signals. Therefore, two TD modules are added in the existing control architecture to acquire the instantaneous values of reference and measured position as well as their first-order derivatives. The structure of the evolved controller is shown in Fig. 5. Corresponding to this evolution, the revised PID control law is given by (14). The error-velocity, $de(t)$, is given by (16).

$$u_1(t) = k_P.e(t) + k_I \int_0^t e(\tau)\, d\tau + k_D.de(t) \tag{14}$$

$$e(t) = \theta_s(t) - \theta_r(t) \tag{15}$$

$$de(t) = \dot{\theta}_s(t) - \dot{\theta}_r(t) \tag{16}$$

4.3 Intelligent feed-forward controller

The intelligent feed-forward controller serves as a supervisory controller. It utilizes an ANFIS that acts as an inverse model to plan and actuate the joint-motor according to the input trajectory pattern (Bakırcıoğlu, 2016).

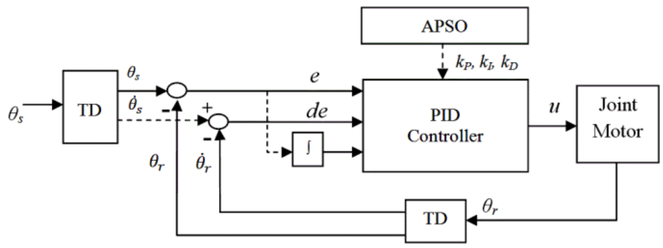

Fig. 5. APSO-tuned PID controller with TD

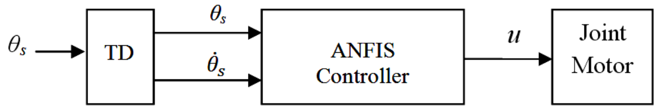

Fig. 6. ANFIS based feed-forward controller

The ANFIS tunes the parameters of the fuzzy inference system using neural network based learning method. The proposed model has two inputs; the finger's joint-angle (θ_s) and its angular-velocity ($\dot{\theta}_s$), as shown in Fig. 6. It integrates the following five-layered ANN with Sugeno-FL structure.

Layer 1: This layer contains the input variables; θ_s and $\dot{\theta}_s$

Layer 2: The second layer fuzzifies the input data using the triangular membership functions (MF) shown in Fig. 7. It evaluates the degree of input in the fuzzy set. The output of the second layer is $\mu_{Ai}(\theta_s)$ or $\mu_{Bi}(\dot{\theta}_s)$. In Fig. 7, the term $\dot{\theta}_s$ is denoted as $d\theta$.

Layer 3: The third layer commences fuzzy inference and produce motor actuation commands based on the fuzzy rule base shown in Table 1. There are a total of 25 rules. The linguistic variables of the input MF of θ_s and $\dot{\theta}_s$as well as the output MF of $\boldsymbol{u_2}$ are defined as; Negative-Big (NB), Negative-Small (NS), Zero (ZE), Positive-Small (PS), and Positive-Big (PB). Each node in this layer corresponds to a rule. The product T-norm aggregation operator is used with each fuzzy neuron.

Layer 4: The fourth layer applies de-fuzzification. The normalized outputs are multiplied by a properly tuned weight factor.

Layer 5: The output layer performs weighted sum of all the outputs incoming from the nodes of layer 4. This linear combination transforms the individual fuzzy classifications into a crisp output, as given by (17).

$$u_2(t) = \frac{\sum_{i=1}^{25} \mu_i (n_i \theta_s + q_i \dot{\theta}_s + s_i)}{\sum_{i=1}^{25} \mu_i} \qquad (17)$$

where, i is the iteration number, and n, q, s are the consequent parameters. The internal structure of the ANFIS is shown in Fig. 8.

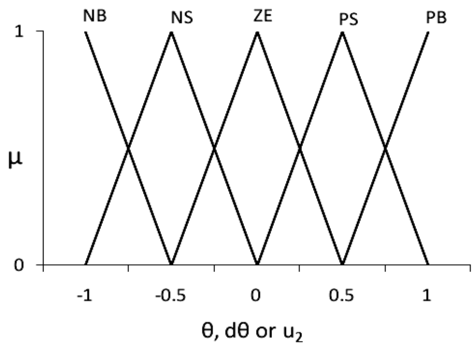

Fig. 7. Input and output membership functions

Table 1. Fuzzy rule base for ANFIS

$\boldsymbol{\theta_s \mid \dot{\theta}_s}$	**NB**	**NS**	**ZE**	**PS**	**PB**
NB	NB	NB	NS	NS	ZE
NS	NB	NS	NS	ZE	M
ZE	NS	NS	ZE	PS	PS
PS	NS	ZE	PS	PS	PB
PB	ZE	PS	PS	PB	PB

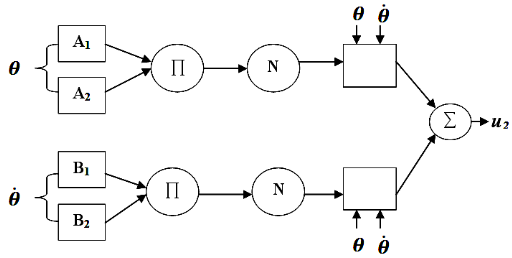

Fig. 8. The ANFIS structure

The hybrid learning algorithm (HLA) is used to train the ANFIS structure (Angulo and Godo, 2007). It consists of the least-squares method (LSM) and the back-propagation algorithm (BPA). The LSM identifies consequent parameters in the forward path. Keeping the consequent parameters fixed, the BPA optimizes the premise parameters iteratively in the backward path, until the desired response is achieved.

4.4 Adaptive combination of controllers

In order to extract the best features of both controllers, the weighted combination of outputs from the ANFIS and PID controller is computed, as shown in (18).

$$u(t) = m \times u_1(t) + (1 - m) \times u_2(t) \qquad (18)$$

Where, m is the weightage of the PID controller existing in the interval [0, 1]. Initially, the weightages are tuned and fixed, at m = 0.647, via trial-and error method. The corresponding control architecture is shown in Fig. 9. However, the hard-coded value of m leads to oscillations in the system's response (demonstrated in Section 5). This issue can be remedied by introducing a smooth non-linear function based adaptation mechanism for the weightages in the existing combination module. The non-linear scaling of the individual control strategies enables the overall control scheme to quickly adapt to variations in system dynamics and improve the tracking accuracy.

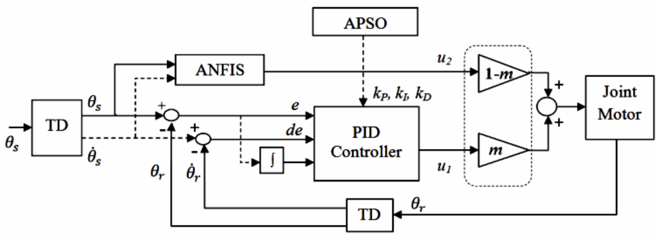

Fig. 9. Collaborative position control mechanism

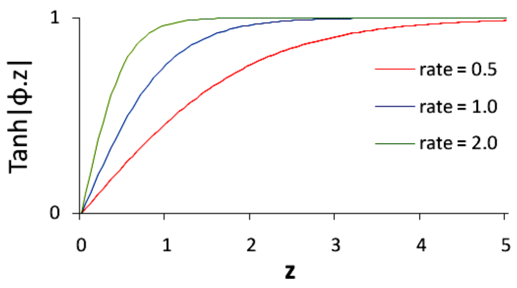

Fig. 10. Hyperbolic tangent function

Therefore, a monotonic non-linear function, bounded between [0, 1], is needed to adaptively change the values of the weightages with respect to variations in the error dynamics of joint-angle. If the error is large, the value of *m* should increase significantly so that the PID controller may contribute a larger control effort to efficiently nullify the error or dampen the oscillations in the response, and vice versa. An abrupt change in the system's state, no matter how small in magnitude, can severely degrade the system's performance. Therefore, the proposed non-linear function should depend on the instantaneous error as well as its derivative. Pertaining to these performance requirements, a hyperbolic-tangent function is chosen to adaptively modulate and combine the two control strategies (Pedroso et al., 2013). The non-linear weightage function is given by (19) and (20).

$$m = tanh\,|\varphi \times z(t)| \tag{19}$$

such that,

$$z(t) = \sqrt{\frac{\hat{e}^2(t) + \widehat{de}^2(t)}{2}} \tag{20}$$

where, φ is the meta-heuristically optimized variation-rate of the HTF. The variation-rate decides the extent of expansion of the HTF as shown in Fig. 10. The term *z(t)* represents the error dynamics. It is root-mean-square of the normalized-values of instantaneous error and its first-derivative. The system is made to track a reference trajectory with PID and ANFIS controller separately, under the influence of artificially induced impulsive bounded perturbations of ± 0.5 rad.

Consequently, the maximum values of *e(t)* and *de(t)* experienced by the system are recorded after each trial. The normalized values of these parameters are evaluated accordingly. The proposed HTF keeps the value of *m* restricted within the interval [0, 1]. With the augmentation of the HTF based adaptation mechanism in the combination module, the control structure evolves into the proposed ACPC mechanism, as shown in Fig. 11.

4.5 Parameter optimization mechanism

The PSO algorithm is a stochastic evolutionary algorithm that provides the optimal values of k_P, k_I, k_D, and φ. It initiates the evolution process by searching for the best-fit solution in random population of candidate solutions, denoted as 'particles'. The algorithm computes and compares the fitness value of a given particle with the best fitness value recorded so far. If a better fitness value is attained as the algorithm progresses, it is set as the new "local-best" (L_b). The particle with highest fitness value among all the particles in the space is chosen as the "global-best" (G_b). An initial search space of 500 candidate particles is taken, in the interval [0, 5], for PSO tuning of the PID parameters as well as the variation-rate. The equations to update the velocity (V_i) and position (X_i) of a particle *'i'* are given in (21) and (22) respectively.

$$V_i = w_i V_i + b_1 r_1 (L_{b,i} - X_i) + b_2 r_2 (\mathrm{G}_b - X_i) \tag{21}$$

$$X_i = X_i + V_i \tag{22}$$

where, b_1 and b_2 are the cognitive coefficients and their values are fixed at 2.12 and 2.01 in this research, respectively. The r_1 and r_2 are random real numbers in the interval [0, 1]. Optimal balancing of inertia weight (*w*) is very important for fast convergence of the swarm towards the best-fit solution. The APSO algorithm used in this paper surpasses the conventional PSO algorithm, since its inertia-weight is adaptively updated (Djoewahir et al., 2013). The values of G_b and L_b are taken and fed back to the adaptive mechanism, as given in (23), to adjust *w*.

$$w_i = w_o - \frac{G_b}{L_{b,i}} \tag{23}$$

where, w_o is the initial value of inertia weight and it is set at 1.25.

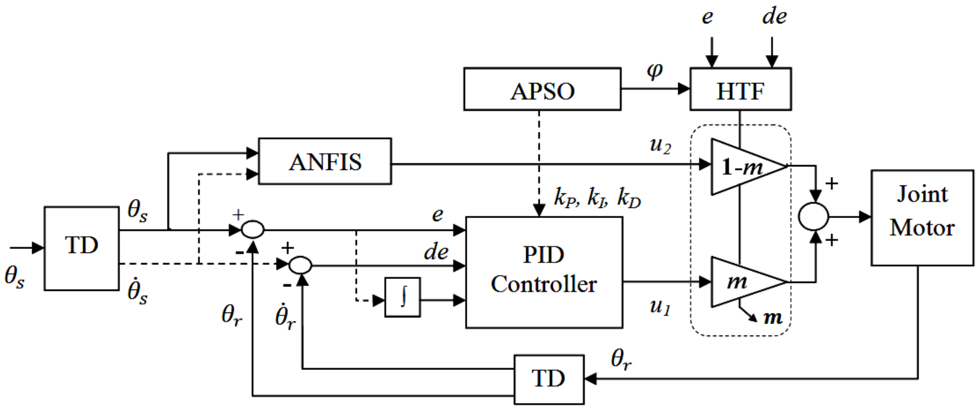

Fig. 11. Adaptive collaborative position control mechanism

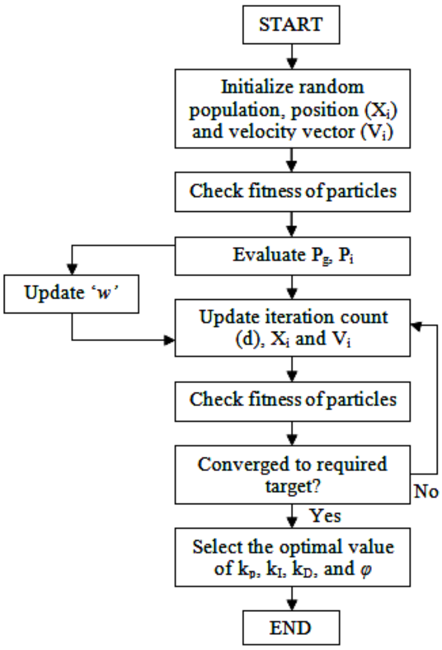

Fig. 12. Flowchart of APSO algorithm

If the particles are far from solution, the ratio of G_b to L_b is less than one. This enlarges the value of w. If the particles are closer to solution, the ratio of G_b to L_b is closer to or equal to one. This lessens the value of w. These adaptive updates tend to increase the convergence rate of the algorithm to quickly provide the best-fit estimate of the above-mentioned parameters. The meta-heuristic optimization algorithm requires a properly defined fitness-function (J). This fitness function is minimized to find the optimal solution. The function used to evaluate the fitness of the particles in this research is given in (24).

$$J = \int_0^t p.e^2(p)\,dp \tag{24}$$

The flowchart of the APSO algorithm is shown in Fig. 12. The optimized values of the PID parameters as well as the variation-rate are provided in Table 2 along with their minimized fitness values. These optimized values are used throughout the experiment.

5. TESTS AND RESULTS

In this section, five different testing scenarios are presented to analyze the performance of the proposed position controller and its previous (or diminished) versions.

Table 2. Optimized parameters

Parameters	Values	min(J)
k_p	3.35	2.53×10^{-4}
k_i	4.58	2.69×10^{-4}
k_d	1.06	4.28×10^{-4}
φ	1.88	5.77×10^{-5}

As discussed previously, the GUI application represents the recorded sensor data graphically for the sake of visualization and comparative assessment. The joint-motor of the index robotic finger of the FFRH is moved with different input trajectories. In the first test-case, the enhancement introduced by the TD in the PID control response is validated. Afterwards, the joint-angle response exhibited by the generic PID controller (as shown in Fig. 5), the generic ANFIS controller (as shown in Fig. 6), the collaborative position controller (CPC) having fixed weightages in the combination module (as shown in Fig. 9), and the adaptive collaborative position controller (ACPC) having HTF based adaptive weightages in the combination module (as shown in Fig. 11) are rigorously analyzed under the influence of different reference trajectory patterns. The corresponding experimental results demonstrated by these controllers are presented for their comparative performance assessment. In all the cases succeeding after the first test, the controllers (PID, ANFIS, CPC, and ACPC) are equipped with TD. In each graphical representation, the applied signals (or the reference trajectory) and the corresponding angular responses demonstrated by the joint-motor are shown in "blue" and "red" color respectively. Once the controllers are tested, their performances are analyzed based on important parameters exhibited by their response; such as rise-time (t_r), overshoot (OS), settling time (t_s), and the root-mean-square of steady-state error (E_{SS}).

Test A: In this test-case, the system's response is analyzed by applying a step-input of 0.873 rad (or 50 degrees). The response with a generic PID controller is shown in Fig. 13. The controller is then enhanced by equipping it with TD modules in the input and the feedback path. The resulting response is shown in Fig. 14. This enhancement significantly reduces the jitter and the noise in the step-response.

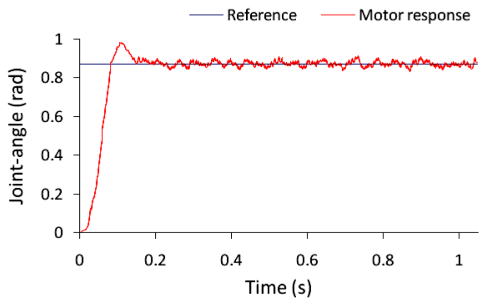

Fig. 13. Step-response of PID controller without TD

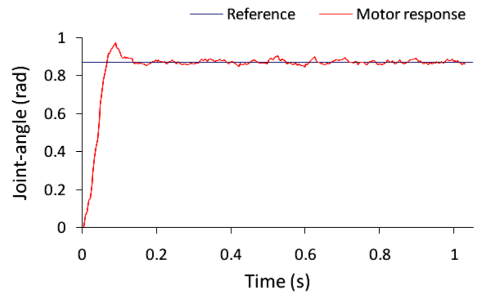

Fig. 14. Step-response of PID controller with TD

Test B: In this test-case, the tracking control performance of the proposed ACPC control strategy is analyzed and compared with its previous versions under the influence of a step-reference. A step-input of 0.873 rad is applied individually to the PID controller, ANFIS, CPC mechanism, and ACPC mechanism. The corresponding responses exhibited by the joint-motor are shown in Fig. 15, 16, 17, and 18, respectively. When the ACPC is responding to the applied step-input signal, the corresponding variation recorded in the value of *m* is shown in Fig 19.

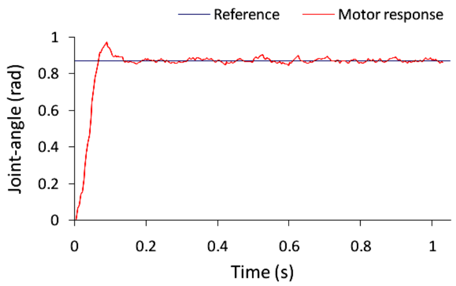

Fig. 15. Step-response with PID controller

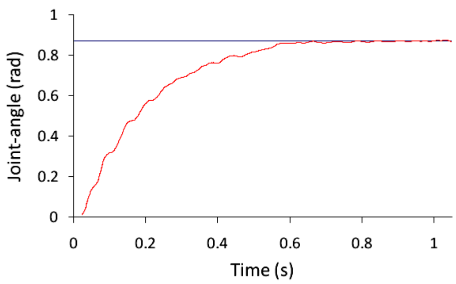

Fig. 16. Step-response with ANFIS

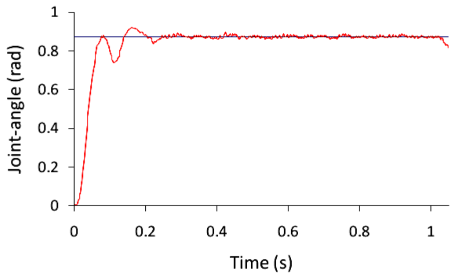

Fig. 17. Step-response with CPC mechanism

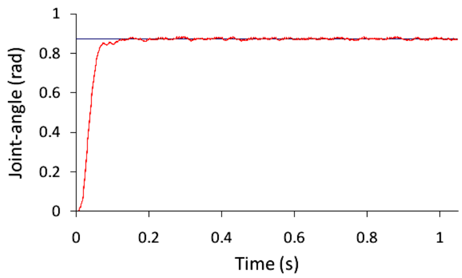

Fig. 18. Step-response with ACPC mechanism

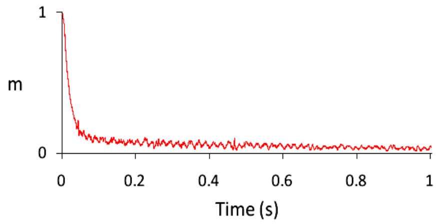

Fig. 19. Variation in value of *m*

Test C: A step-input of 0.873 rad is applied again to the four control mechanisms. The reference-input is perturbed by the application of a bounded impulsive disturbance signal. The amplitude and duration of the applied disturbance signal is ±0.35 rad and 4.0 ms, respectively. The controller's ability to mitigate the effect of perturbation is analyzed by the maximum absolute error (*MAE*) incurred in the response and the time taken by the response to recover (t_{rec}) and converge within ±2% of reference value. The responses of the generic PID controller and its evolved variants are shown in Fig. 20, 21, 22, and 23, respectively. As the proposed controller responds to the perturbed input signal, the corresponding variation in the value of *m* is shown in Fig 24.

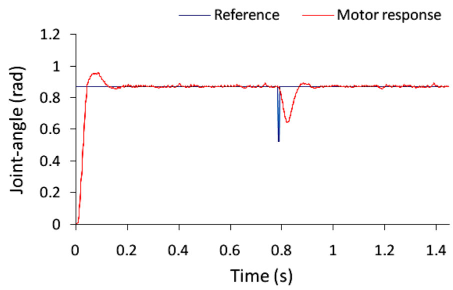

Fig. 20. Step-response with PID controller

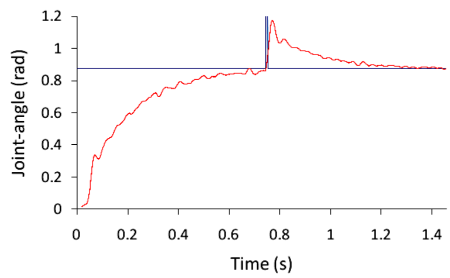

Fig. 21. Step-response with ANFIS

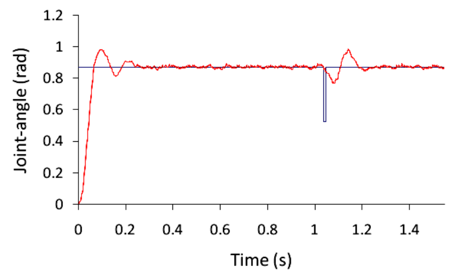

Fig. 22. Step-response with CPC mechanism

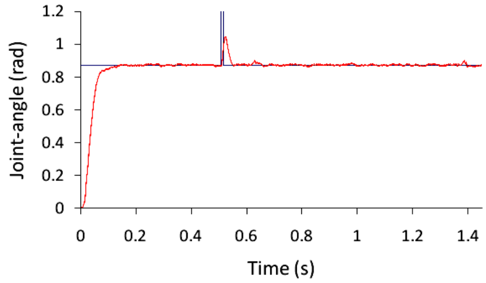

Fig. 23. Step-response with ACPC mechanism

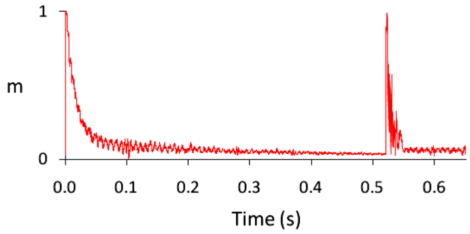

Fig. 24. Variation in value of *m*

Test D: In this case, the system's response is tested by applying a square-wave trajectory pattern that swings between 0.35 rad and 1.40 rad, at a frequency of 0.4 Hz. The reference trajectory is applied to the four control strategies. The responses of the generic controller and its evolved variants are shown in Fig. 25, 26, 27, and 28, respectively.

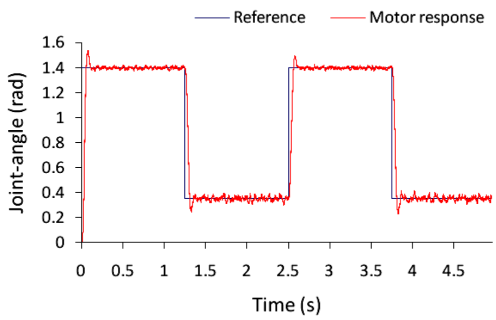

Fig. 25. Square-wave response with PID controller

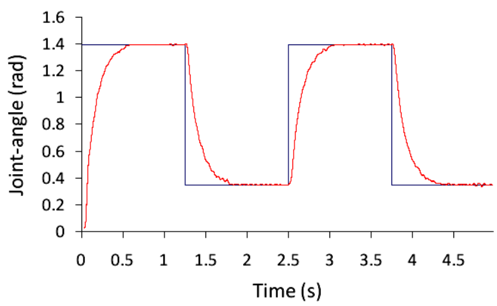

Fig. 26. Square-wave response with ANFIS

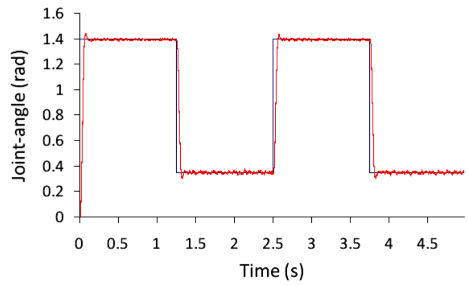

Fig. 27. Square-wave response with CPC mechanism

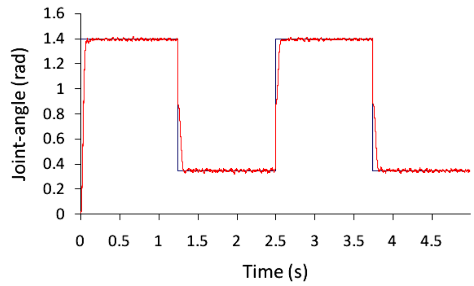

Fig. 28. Square-wave response with ACPC mechanism

Test E: In this case, the system's response is tested by applying a triangular trajectory pattern that swings linearly between 0.35 rad. and 1.40 rad., at a frequency of 0.4 Hz. The reference trajectory is applied to the four control strategies. The responses of the generic controller and its evolved variants are shown in Fig. 29, 30, 31, and 32, respectively.

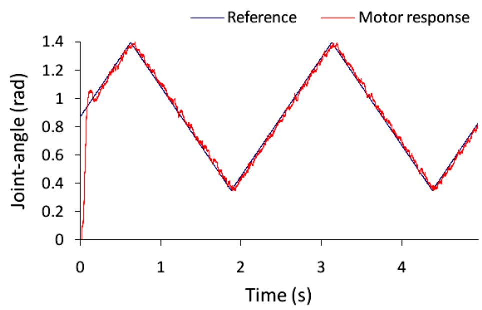

Fig. 29. Triangular-wave response with PID controller

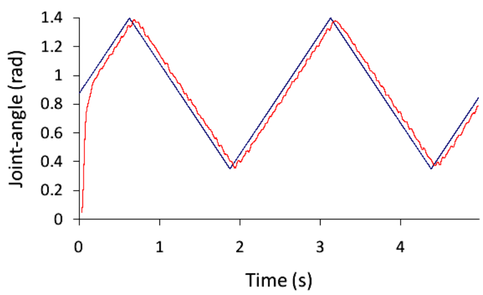

Fig. 30. Triangular-wave response with ANFIS

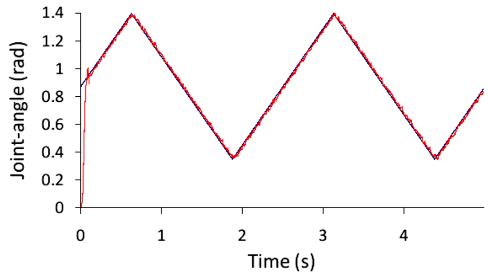

Fig. 31. Triangular-wave response with CPC mechanism

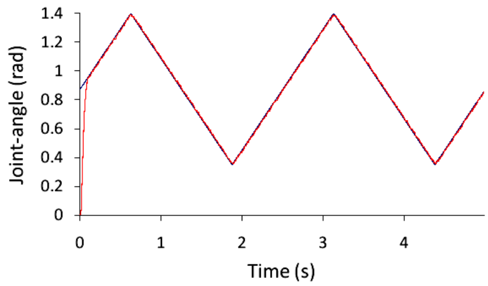

Fig. 32. Triangular-wave response with ACPC mechanism

The important performance parameters are inferred from graphical response recorded for each of the four control strategies, under the five testing scenarios (A to E). The result is presented in Table 3. The experimental results clearly manifest that the proposed control mechanism is superior in performance than its previous (diminished) versions.

6. CONCLUSION

The synthesis of an adaptive collaborative position and tracking controller for the finger joint of a FFRH is described in this paper. The ANFIS controller in the feed-forward loop is trained to accurately track the trajectory pattern. The disturbance rejection and transient response improvement is done via the PID controller. The tracking-differentiator is also incorporated with the controller to improve the differential signal quality. The individual controller outputs are fused together via a weighted summing module. The weightages are determined via a smooth non-linear bounded HTF. The dynamic non-linear modulation of individual controller outputs enhances the reflexes of robotic fingers and improves the overall response of the revolute joint for time-varying reference trajectories. It efficiently nullifies the tracking errors and increases the rate of error-convergence in the presence of bounded disturbance signals. The experimental results in Table 3 validate the robustness and efficacy of proposed ACPC mechanism. The response-graphs clearly demonstrate that the proposed strategy, that employs HTF-assisted weighted combination of PID and ANFIS control outputs, offers superior position and tracking control performance for the robotic manipulator. In future, apart from non-linear gain functions, fuzzy inference and neural network based coupling methodologies can also be explored. Model-based optimal controllers can also be analyzed and integrated with the existing system to improve its response.

Table 3. Summary of experimental results

Test	**Controller**	t_r (s)	**OS** (%)	t_s (s)	$E_{ss} \times 10^{-3}$ (rad)	t_{rec} (s)	**MAE** (rad)
A	PID$_{(\text{No TD})}$	0.13	13.0	0.17	14.81	-	-
	PID$_{(\text{TD})}$	0.11	8.0	0.18	7.39		
B	PID	0.11	8.0	0.18	7.39	-	-
	ANFIS	0.61	0.3	0.63	1.36		
	CPC	0.10	5.3	0.25	3.52		
	ACPC	0.08	0.2	0.14	1.48		
C	PID	0.10	8.6	0.18	6.42	0.13	0.196
	ANFIS	0.62	0.0	0.65	2.51	0.54	0.490
	CPC	0.09	8.4	0.22	3.47	0.21	0.178
	ACPC	0.08	0.1	0.14	1.42	0.06	0.173
D	PID	0.10	9.1	0.17	5.22	-	-
	ANFIS	0.60	0.0	0.62	1.18		
	CPC	0.08	5.8	0.16	3.69		
	ACPC	0.08	0.0	0.15	1.52		
E	PID	0.10	9.3	0.21	4.98	-	-
	ANFIS	0.60	0.0	0.71	5.37		
	CPC	0.09	4.1	0.26	3.24		
	ACPC	0.07	0.0	0.13	1.12		

REFERENCES

Angulo, C., Godo, L. (2007). *Artificial intelligence research and development*. IOS Press, Amsterdam, Netherlands.

Abdallah, M.E., Platt Jr., R., and Wampler, C.W. (2013). Decoupled torque control of tendon-driven fingers with tension management. *The International Journal of Robotics Research*, 32(2), pp. 247-258.

Anbarasi, S., and Muralidharan, S. (2016). Enhancing the Transient Performances and Stability of AVR System with BFOA Tuned PID Controller. *Control Engineering and Applied Informatics*, 18(1), pp. 20-29

Bakırcıoğlu, V., Sen, M.A., Kalyoncu, M. (2016). Adaptive Neural-Network Based Fuzzy Logic (ANFIS) Based Trajectory Controller Design for One Leg of a Quadruped Robot. In: *Proceedings of the 5th International Conference on Mechatronics and Control Engineering*, Venice, Italy, pp. 82-85.

Bequette, B.W. (2003). *Process Control: Modeling, Design, and Simulation*, pp. 195-209. Prentice Hall, New Jersey, USA.

Bhatti, O.S., Mehmood-ul-Hassan, K., and Imtiaz, M.A. (2015). Attitude Control and Stabilization of a Two-Wheeled Self-Balancing Robot. *Control Engineering and Applied Informatics*, 17(3), pp. 98-104.

Biswas, P., Maiti, R., Kolay, A., Sharma, K.D., and Sarkar, G. (2014). PSO based PID controller design for twin rotor MIMO system. In: *Proceedings of 2014 International Conference on Control, Instrumentation, Energy and Communication*, Kolkata, India, pp. 56-60.

Carbone, G., and Ceccarelli, M. (2008). DESIGN OF LARM HAND: PROBLEMS AND SOLUTIONS. *Control Engineering and Applied Informatics*, 10(2), pp. 39-46.

Carbureanu, M. (2014). The Development of a Neuro-Fuzzy Expert System for Wastewater pH Control. *Control Engineering and Applied Informatics*, 16(4), pp. 30-41

Chen, C.H., and Naidu, D.S. (2011). Fusion of fuzzy logic and PD control for a five-fingered smart prosthetic hand. In: *Proceedings of 2011 IEEE International Conference on Fuzzy Systems*, Taipei, Taiwan, pp. 2108-2115.

Chen, C.H., and Naidu D.S. (2013). Hybrid control strategies for a five-finger robotic hand. *Biomedical Signal Processing and Control*, 8(4), pp. 382-390.

Chen, C.H., Ze, Y., and Li, C. (2012). Mechatronics design of multi-finger robot hand. In: *Proceedings of 12th International Conference on Control, Automation and Systems*, Jeju Island, South Korea, pp. 1491 -1496.

Devaraj, J.A. (2015). Adaptive Particle Swarm Optimization based System Identification and Internal Model Sliding Mode controller for Mass Flow System. *Control Engineering and Applied Informatics*, 17(4), pp. 3-13.

Djoewahir, A., Tanaka, K., and Nakashima, S. (2013). Adaptive PSO-based self-tuning PID controller for ultrasonic motor. *International Journal of Innovative Computing, Information and Control*, 9(10), pp. 3903-3914.

Duka, A.V. (2015). ANFIS Based Solution to the Inverse Kinematics of a 3DOF Planar Manipulator. *Procedia Technology*, 19, pp. 526-533

Elmerabete, J., Li, H., and Rafi, Y. (2010). Application of Real-Time Control System Using LabVIEW in Distance-Learning. In: *Proceedings of 2010 International Conference on Measuring Technology and Mechatronics Automation*, Shanghai, China, pp. 663-666.

Ghosh, A., and Banerjee, S. (2015). Control of Switched-Mode Boost Converter by Using Classical and Optimized Type Controllers. *Control Engineering and Applied Informatics*, 17(4), pp. 114-125.

Guo, B., Hu, L., and Bai, Y. (2012). A nonlinear PID controller with tracking differentiator applying in BLDCM servo system. In: *Proceedings of 2012 7th International Power Electronics and Motion Control Conference*, Harbin, China, pp. 2467-2471.

Jimenez-Uribe, A., Serna-Hernandez, L.F., Hernandez-Paredes, J.M., Munoz-Baron, B. (2015). Comparative Study of a PID and PD Control Bounded by Hyperbolic Tangent Function in Robot 3 DOF. In: *Proceedings of 2015 International Conference on Mechatronics, Electronics and Automotive Engineering*, Cuernavaca, Mexico, pp. 199-204.

Jun, S., and Huiqiang, C. (2015). Rotary position system based on improved nonlinear tracking differentiator-fuzzy PID. In: *Proceedings of 2015 34th Chinese Control Conference*, Hangzhou, China, pp. 5521-5526.

Medewar, P.G., and Munje, R.K. (2015). PSO based PID controller tuning for PMDC motor. In: *Proceedings of 2015 International Conference on Energy Systems and Applications*, Pune, India, pp. 522-526.

Niehues, T., Badger, J., Diftler, M., and Ashish, D.D. (2014). Cartesian-space control and dextrous manipulation for multi-fingered tendon-driven hand. In: *Proceedings of 2014 IEEE International Conference on Robotics and Automation*, Hong Kong, China, pp. 6777-6783.

Pedroso, M.D., Nascimento, C.B., Tusset, A.M., and Kaster, M.S. (2013). A Hyperbolic Tangent Adaptive PID + LQR Control Applied to a Step-Down Converter Using Pole-Placement Desing Implemented in FPGA. *Mathematical problems in Engineering*, 2013, pp. 1-8.

Potluri, C., Kumar, P., Anugolu, M., Chiu, S., Urfer, A., Schoen, M.P., and Naidu, D.S. (2010). sEMG based fuzzy control strategy with ANFIS path planning for prosthetic hand. In: *Proceedings of 2010 3rd IEEE RAS and EMBS International Conference on Biomedical Robotics and Biomechatronics*, Tokyo, Japan, pp. 413-418.

Rezaeeian, A., Shasti, B., Doosthoseini, A., Yousefi-Koma, A. (2008). ANFIS modeling and feed forward control of shape memory alloy actuators. In: *Proceedings of the 10th WSEAS International Conference on Automatic Control, Modelling & Simulation*, Istanbul, Turkey, pp. 243-248.

Saini, S., and Rani, S. (2012). Temperature Control Using Intelligent Techniques. In: *Proceedings of 2012 Second International Conference on Advanced Computing & Communication Technologies*, Rohtak, India, pp. 138-145.

Salim, S.N.S., Rahmat, M.F., Faudzi, A.A.M., Ismail, Z.H., Sunar, N.H., and Samsudin, S.A. (2014). Robust Control Strategy for Pneumatic Drive System via Enhanced Nonlinear PID Controller. *International Journal of Electrical and Computer Engineering*, 4(5), pp. 658-667.

Seraji, H. (1998). A New Class of Nonlinear PID Controllers with Robotic Applications. *Journal of Robotic Systems*, 15(3), pp. 161-181.

Sharma, R., Gaur, P., and Mittal, A.P. (2016). An enhanced hybrid fuzzy logic controller for robotic manipulator. In: *Proceedings of 2016 3rd International Conference on Computing for Sustainable Global Development*, New Delhi, India, pp. 2465-2470.

Shauri, R.L.A., Salleh, N.M., and Hadi, A.K.A. (2014). PID position control of 7-DOF three-fingered robotic hand for grasping task. In: *Proceedings of 2014 IEEE International Conference on Control System, Computing and Engineering*, Penang, Malaysia, pp. 70-74.

Su, Y.X., Sun, D., and Duan, B.Y. (2005). Design of an enhanced nonlinear PID controller. *Mechatronics*, 15, pp. 1005-1024.

Vijayakumar, K., and Manigandan, T. (2016). Nonlinear PID Controller Parameter Optimization using Enhanced Genetic Algorithm for Nonlinear Control System. *Control Engineering and Applied Informatics*, 18(2), pp. 3-10.

Widhiada, W., Nindhia, T.G.T., and Budiarsa, N. (2015). Robust Control for the Motion Five Fingered Robot Gripper. *International Journal of Mechanical Engineering and Robotics Research*. 4(3), pp. 226-232.

Xu, Z., Kumar, V., Matsuoka, Y., and Todorov, E. (2012). Design of an anthropomorphic robotic finger system with biomimetic artificial joints. In: *Proceedings of 2012 4th IEEE RAS & EMBS International Conference on Biomedical Robotics and Biomechatronics*, Rome, Italy, pp. 568 - 574.

Yu, H., and Honglun, W. (2015). Application of Tracking-Differentiator in Angular Measurements on Spinning Projectiles Using Magnetic Sensors. In: *Proceedings of 2015 7th International Conference on Intelligent Human-Machine Systems and Cybernetics*, Hangzhou, Zhejiang, China, pp. 433-436.

Zaki, A.M., Soliman, A.M., Mahgoub, O.A., and El-Shafei, A.M. (2010). Design and implementation of efficient intelligent robotic gripper. In: *Proceedings of 2010 International Conference on Modelling, Identification and Control*, Okayama City, Japan, pp. 710-716.